ACS OMEGA

http://pubs.acs.org/journal/acsodf

Article

Effect of High-Energy Milling on the Dissolution of Anti-HIV Drug Efavirenz in Different Solvents

Narges Ataollahi,* Marica Broseghini, Fabio F. Ferreira, Alberto Susana, Massimo Pizzato, and Paolo Scardi

Cite This: *ACS Omega* 2021, 6, 12647−12659

Read Online

ABSTRACT: The anti-HIV drug efavirenz (EFV) displays low and variable bioavailability because of its poor aqueous solubility. Ball milling is a simple and cost-effective alternative to traditional micronization to improve the solubility and dissolution rate of EFV. A multibody dynamics model was employed to optimize the milling process parameters, while the motion of the balls in the mill jar was monitored *in operando*. This led to a better understanding of the milling dynamics for efficient comminution and enhancement of EFV dissolution. The variability of results for different EFV batches was also considered. Depending on the EFV batch, there were intrinsic differences in how the milling affected the dissolution behavior and inhibition of HIV-1 infection. High-energy grinding is more effective on EFV materials containing an amorphous fraction; it helps to remove agglomeration and enhances dissolution. Polyvinylpyrrolidone (PVP) addition improves the dissolution by forming a hydrophilic layer on the EFV surface, thereby increasing the drug wettability. Polymorphism also affects the quality, dosage, and effectiveness of the drug. The mechanical stress effect and PVP addition on the EFV polymorphic transformation were monitored by X-ray powder diffraction, while the residual of ground EFV was collected after dissolution, analyzed by scanning electron microscopy, and provided insights into the morphological changes.

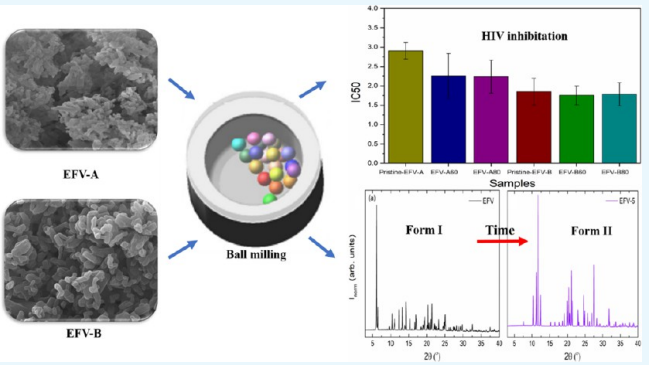

1. INTRODUCTION

Efavirenz (EFV) is a reverse transcriptase inhibitor known for the treatment of human immunodeficiency virus (HIV) infection.[1−3] The solubility of a drug substance is one of the significant parameters impacting absorption[4] as well as bioavailability, defined as the fraction of the administered dose of a drug that enters the systemic circulation, thereby accessing the site of action.[5] It is reported that EFV has a low aqueous solubility (9.2 μg mL^{-1}) (pH 8.7) at 25 °C,[6−8] higher as the pH increases above 9, for the proton loss on the carbamate group's amine.[6] Unfortunately, EFV tends to be eliminated in the human systemic circulation before the dissolution and absorption into the systemic circulation processes are completed, therefore requiring an increased dosage to achieve therapeutic levels in the body, often implying adverse effects for the patient.[9−11] Several approaches to improve EFV dissolution were reported using various carriers, including biosources[12] or synthetic routes.[13,14] These carriers have interesting properties, including solubility in water and in a broad range of liquid media, unique wetting, high chemical and thermal resistance, biocompatibility, and the absence of toxicity, all necessary for different applications as biomaterials, for medical and nonmedical uses.[15] Chemical and physical modifications of the compounds have also been explored to overcome the limitation of poor solubility. While the former route implies the design of new polymorphs often followed by undesirable alterations of the biological effect, the latter keeps it unchanged, requiring consequently a smaller amount of *in vitro* and *in vivo* testing procedures.

The chemical methods such as PEGylation,[13] spray-drying,[10,16] and hot-melt[17,18] proved to have promising therapeutic potential. However, it is essential to consider their limitations, including the need for expensive equipment, particularly the parameters optimization, critical to obtain a stable and reproducible nanosuspension with a uniform distribution. One of the most common physical methods to enhance drug solubility is particle size reduction.[19−21] This aims at increasing the surface area in contact with the dissolution medium, S, which is proportional to the dissolution rate, dC/dt, as stated by the Nernst−Brunner equation[22]

Received: February 8, 2021
Accepted: April 19, 2021
Published: May 3, 2021

$$\frac{dC}{dt} = \frac{DS}{Vh}(C_s - C) \quad (1)$$

where D is the diffusion coefficient, V is the volume of the dissolution medium, h is the diffusion layer thickness, C_s is the saturation solubility, and C is the instantaneous concentration at time t.

Different technologies are available for the production of ultrafine particles,[23,24] and micronization is the most widely used by the pharmaceutical industry, employing, in particular, air-jet mills.[10,19,25] Instead, ball milling exploits high-energy impacts and mechanical attrition for comminution and disaggregation of particles and enhances the dissolution rate of a drug.[3,26] Apart from size reduction, milling can induce alterations of the drug particles (e.g., shape, roughness, structural disorder, and defect content) that have a considerable impact on dissolution, as revealed by several studies.[3,11,19,26] Therefore, to completely understand the phenomenon, the connections with particle size and other physicochemical parameters should be investigated.

Since the end-product characteristics strongly relate to the milling parameters, the application of a multibody dynamics model of the planetary ball mill, also supported by camera recordings of the process, was crucial to predict the mill configuration providing with the more significant reduction of particle size, possibly leading to a faster and complete dissolution. Polyvinylpyrrolidone (PVP) was chosen as a carrier because of its historical safety use in pharmaceutical formulations and capability to prevent agglomeration; moreover, the influence of distilled water and methanol on the dissolution behavior of ground samples was investigated.

To completely understand the dissolution phenomenon, the morphology, the vibrational spectra of as-milled samples, and their residuals after the dissolution test were studied by scanning electron microscopy (SEM), transmission electron microscopy (TEM), and Fourier transform infrared spectroscopy (FTIR). The mechanical grinding effects and PVP on EFV's polymorphic transformation were monitored by X-ray powder diffraction (XRPD). Finally, the *in vitro* antiviral activity of EFV samples was evaluated.

2. RESULTS AND DISCUSSION

The solubility is strongly influenced by the presence and quantity of agglomerated and dense particles in the raw EFV. Different batches of pristine EFV have shown different dissolution behaviors, even though they were produced under the same nominal conditions for synthesis, and the pristine materials available in the market present the same structure. The XRPD pattern of pristine EFV (Figure 1) shows that batch B, with sharper Bragg peaks and a lower diffuse signal, is well-crystalline compared to batch A.

In general, the dissolution profile of raw materials shows poor solubility in distilled water with respect to methanol (40 wt %), as displayed in Figure 2. However, batch B shows a slightly higher dissolution rate, both in distilled water and in methanol. The comparison of residual weight between batch A and B shows that the amount of dissolved drug in B is greater than in A for both dissolution media (Table SI-3). This can be related to the batch B morphology (Figure 3b,d), which is significantly less agglomerated and well-crystalline with respect to batch A (Figure 3a,c). This observation finds a possible explanation in the different pharmaceutical grades of the two batches. Batch A has been exposed to the environment for a longer period compared with batch B; hence, the quality of EFV raw materials influences the dissolution of EFV drug.

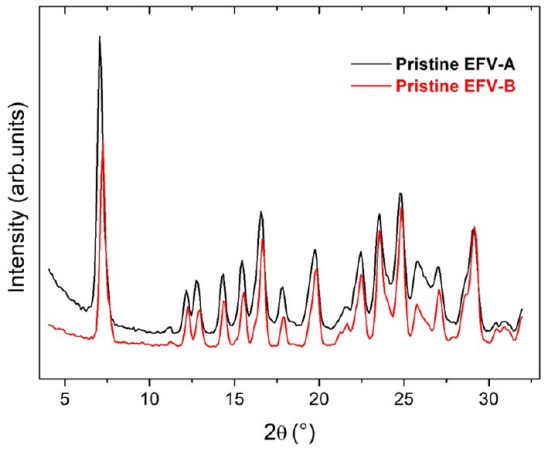

Figure 1. XRPD patterns (Co Kα radiation λ = 1.7889 Å) of pristine EFV (batches A and B).

A series of preliminary experimental tests were performed by milling EFV (batch A) for 30 min under conditions typical for ceramic materials and metals, namely, Ω = 200 rpm and as $\omega/\Omega + 1 = -1$ and -3.4. XRPD line profile analysis (LPA) on the end products revealed that the process had little effect on the crystalline domain size (Figure 4a). This condition appeared to be too energetic, to the point of causing the recrystallization of the material, and the formation of a different polymorph and partial amorphization, demonstrated by the larger diffuse scattering signal in the XRPD pattern (Figure 4b).

When the milling process lasts for too long, recrystallization leads to a different morphology, with thin needles on large lumps of the agglomerate material, clearly visible in the SEM micrographs of Figure 5.

A detailed XRDP study was performed on the EFV (batch B) ground with a mixer mill (MM400) at 25 Hz for 5 min with a waiting time of 3 min until reaching 30 min. The purpose was to investigate what phenomena occur in highly energetic conditions; the results are illustrated in Figure 6. Pristine EFV shows crystalline form I (CSD AJEYAQ02),[27] based on the Crystallographic Structural Database system.[28]

Rietveld refinements (Figure 7) were carried out using the software TOPAS-Academic v7.[29] For all samples, the background was fitted using a 59-term Chebyshev function. The unit cell parameters, isotropic displacement parameters, and an 8-term spherical harmonics function to account for the crystallites' preferred orientation were refined. The fitting results are reported in Table SI-1.

The pristine EFV sample is highly crystalline in comparison to the ball-milled samples. The addition of PVP to the EFV sample promoted the complete amorphization of the sample, which was kept even after 1 week (Figure SI-1). PVP seems to interact with the EFV sample, thus avoiding its crystalline rearrangement. On the other hand, in the case of the pure EFV sample subjected to the ball milling process, the EFV polymorphic form II (CSD AJEYAQ01)[30] gradually appeared with time (Figure 6c−f).

The EFV sample measured after being subjected to the ball-milling process (EFV-1) revealed form I's maintenance but with a significant amount of an amorphous contribution. The degree of crystallinity (DoC)[31] was calculated to be ∼53.10 wt % (Figure 8a). The same sample was measured after increasing

https://doi.org/10.1021/acsomega.1c00712
ACS Omega 2021, 6, 12647−12659

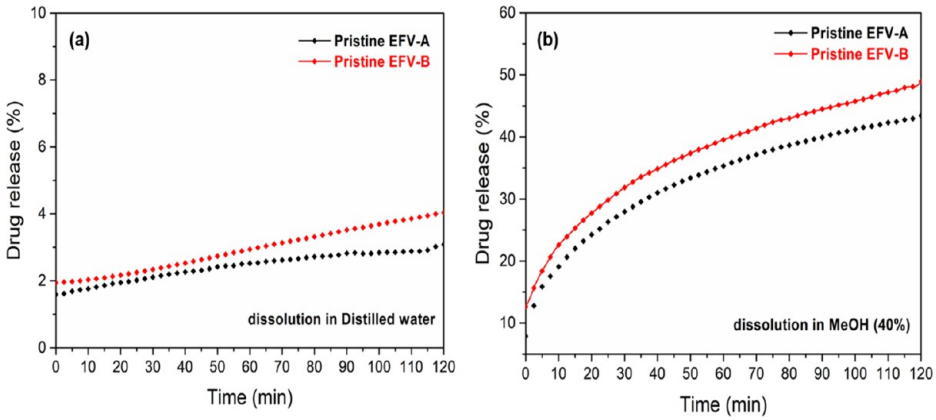

Figure 2. Dissolution profile of pristine EFV (batches A and B): (a) in distilled water and (b) in methanol.

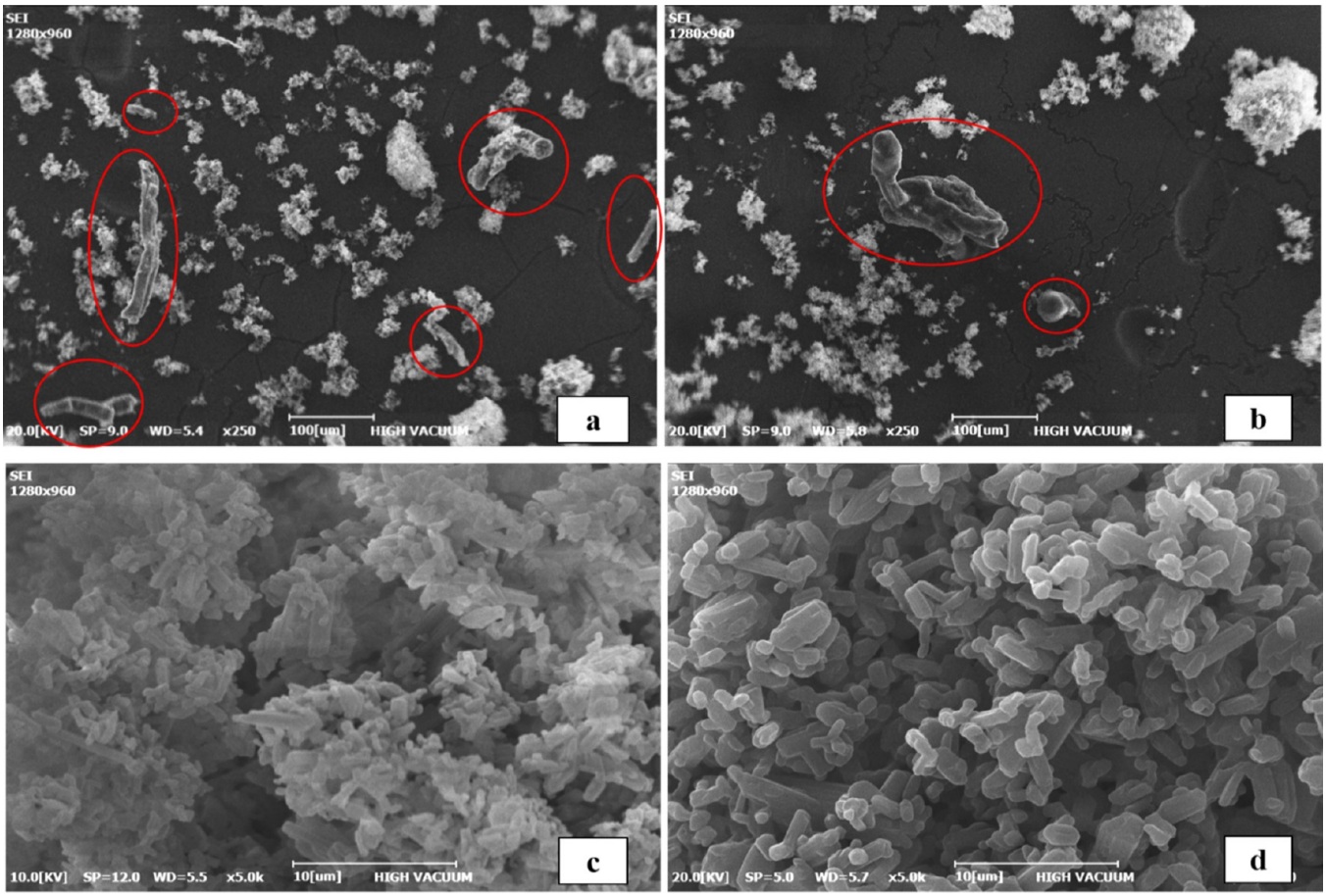

Figure 3. SEM image of pristine EFV with different magnifications of ×250 and ×5.0k: batch A (a, c) and batch B (b, d). Red circles are pointing at the dense and agglomerated particles.

time (7 days (EFV-2), 14 days (EFV-3), 30 days (EFV-4), and 60 days (EFV-5)). A quantitative phase analysis (QPA)[32] by the Rietveld method (Figure 8, more details in Figure SI-2) showed a significant evolution of form II from 9 to 77 wt % after 30 days. Finally, after 60 days, EFV-1 was entirely transformed into form II (EFV-5), as shown in Figure 8c. These observations demonstrate that polymorphism is correlated with time and occurs if the milling process is not performed correctly. It is worth noting that Figure 8d displays only the corresponding crystalline phase mass fraction(s). The DoC indicated the following amounts of amorphous contribution to each sample: EFV = 1.8%, EFV-1 = 46.9%, EFV-2 = 50.3%, EFV-3 = 28.1%, EFV-4 = 76.5%, and EFV-5 = 12.0%.

EFV is a delicate material where the extreme grinding condition involves attrition and heat, resulting in amorphization, recrystallization, polymorph transformation, agglomeration, and finally, leading to a poor dissolution, as shown in Figure SI-3. Therefore, the model and camera recordings *in operando* were applied as a helpful support in the milling process comprehension to set up conditions suitable to EFV. As a first step, energy reduction was pursued. Ω = 60 rpm and

https://doi.org/10.1021/acsomega.1c00712
ACS Omega 2021, 6, 12647−12659

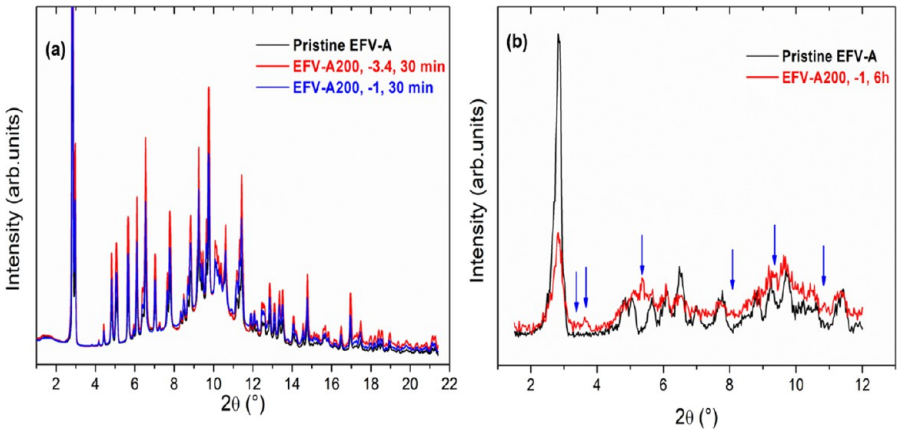

Figure 4. XRPD patterns (Mo Kα radiation λ = 0.7093 Å) of pristine and milled EFV with Ω = 200 rpm and $\omega/\Omega + 1 = -1$ and -3.4, milling time: 30 min (a). For longer milling time (b) (EFV-Ω = 200 rpm and $\omega/\Omega + 1 = -1$, milling time: 6 h). Arrows correspond to the supplementary peaks in EFV-200, −1, 6 h (different polymorph).

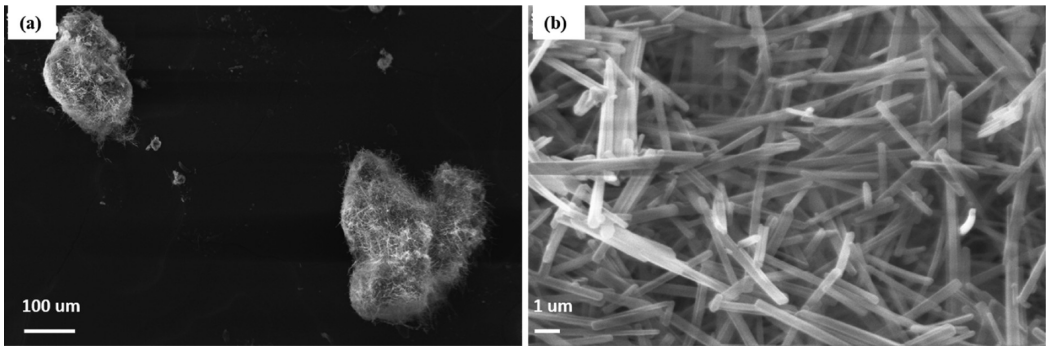

Figure 5. SEM micrographs of EFV with an extreme grinding condition (Ω = 200 rpm and as ω/Ω −1 and −3.4, milling time: 6 h) with a different magnification of ×200 (a) and ×10.0 k (b).

Ω = 80 rpm were tested both for the zirconium−zirconium, and zirconium−EFV interactions and simulations were performed varying the $\omega/\Omega + 1$ velocity ratio between 0 and −4.6 besides a remarkable global reduction of the magnitude of the average stress energy with respect to Ω = 200 rpm. Figure 9 shows the maximum of this quantity to range between approximately $\omega/\Omega + 1 = -3.0$ and -3.8 for both the tested Ω.

Indeed, it was shown that the maximum energy corresponds to the largest disorder in balls motion, also providing with the more significant amount of high normal velocity impacts, deemed as the most effective in comminution. The maximum complexity of balls movements was confirmed to arise around $\omega/\Omega + 1 = -3.4$ by the visual inspection of ball trajectories both in simulations and camera recordings, as reported in Figure10, pointing out also a good agreement between images obtained from these two techniques.

High-energy grinding positively affects the dissolution behavior of EFV (batch A) with Ω = 60 and 80 rpm, as shown in Figure 11a,b. Milling with a main disk speed of Ω = 80 rpm (EFV-A80) shows better solubility in distilled water and methanol compared to EFV-A60 (Ω = 60 rpm). These samples dissolution profiles demonstrate that the optimized milling conditions (reduction of Ω) lead to improved dissolution behavior, resulting in a better biopharmaceutical performance with respect to the preliminary test (Figure SI-3). However, the reduction of Ω is ineffective on the dissolution behavior of batch B. The dissolution of as-milled samples (EFV-B60 and EFV-B80) is lower compared with the pristine EFV regardless of main disk speed (Ω = 60 and Ω = 80 rpm) and dissolution media (distilled water and methanol) (Figure 11c,d). This shows that the structure and morphology of pristine EFV have an important role in the milling process's effect. High-energy grinding is more effective on EFV materials containing a fraction of the amorphous phase (batch A) since it removes agglomeration and enhances the dissolution. Basically, if the pristine EFV is well-crystalline (batch B), the milling can cause recrystallization, forming agglomerations and resulting in lower dissolution.

To assess the morphology's insight, the residues of as-milled EFV, deposited at the bottom of the dissolution vessel, were collected and dried at room temperature and then observed by SEM. A correlation between the weight of the residual (Table SI-2) and dissolution can be found: the lower the residual weight, the higher the dissolution. The residual in distilled water (Figure 12c,d) demonstrated no significant alteration in the morphology compared to the as-milled sample (Figure 12a,b). Changes in size and shape of crystals are more evident in EFV samples' residues (EFV-A60 and EFV-A80) in methanol (Figure 12e,f). The rod-shaped crystal is transformed into a needle-like crystal distributed in all parts of particles, proving that EFV contains polymorphs with different reactions toward the solvent.

The morphology trend in the residuals of as-milled samples in batch B (Figure 13a−c and Figure SI-4) is different compared with A, in particular, the shape of residues and formation of the dense particle during the milling process. In

https://doi.org/10.1021/acsomega.1c00712
ACS Omega 2021, 6, 12647−12659

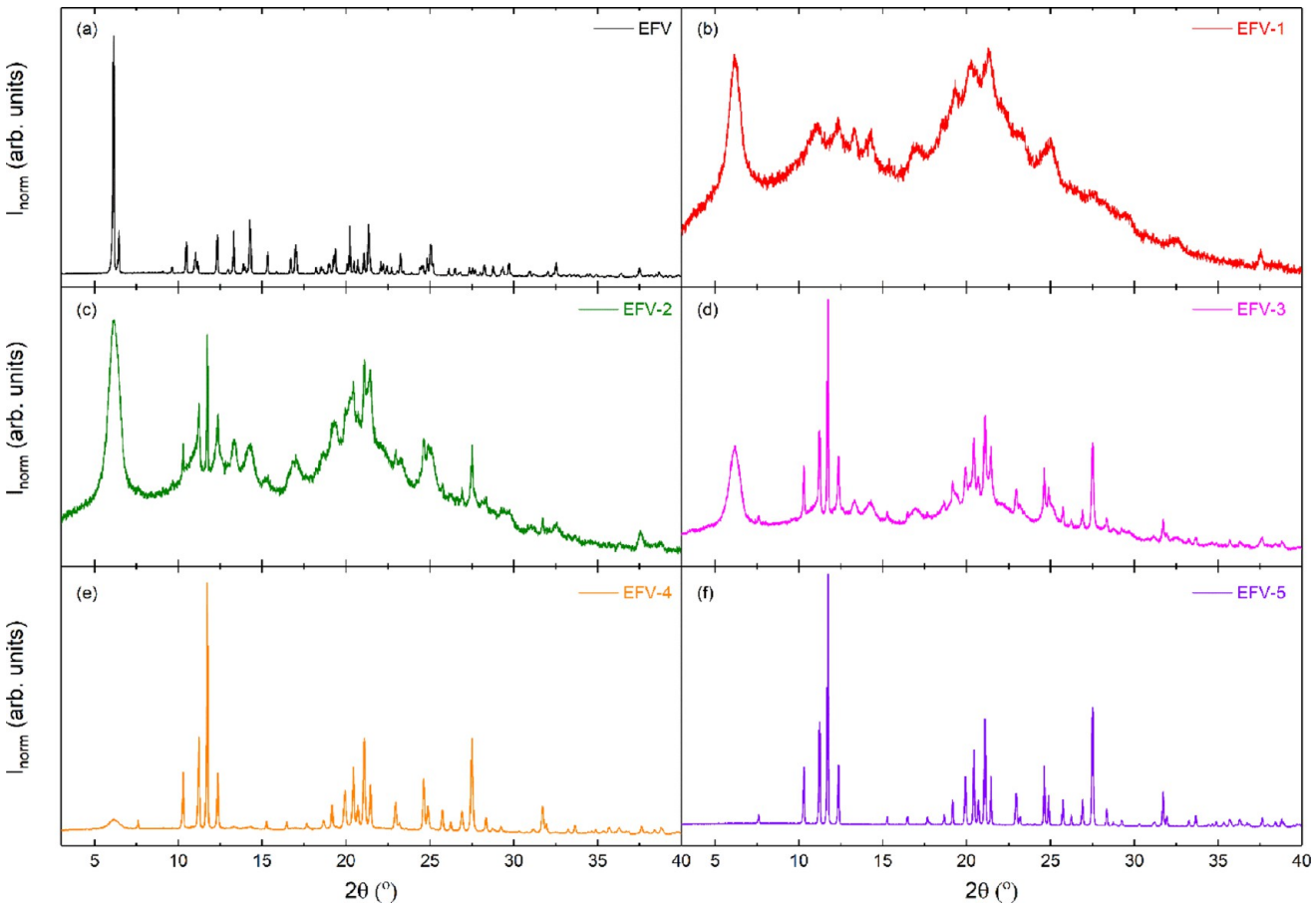

Figure 6. XRPD patterns (Cu Kα radiation (λ = 1.54056 Å)) of (a) pristine EFV and ball-milled samples: (b) EFV-1 (as grinded), (c) EFV-2 (after 7 days), (d) EFV-3 (after 14 days), (e) EFV-4 (after 30 days), and (f) EFV-5 (after 60 days).

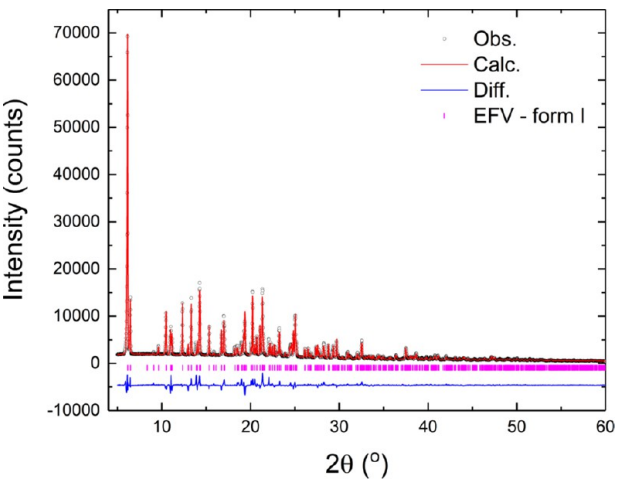

Figure 7. Rietveld plot of the pristine EFV sample. The black circles represent the observed pattern, while the red curve indicates the calculated one. The blue line at the bottom displays the difference between the observed and calculated patterns. The magenta vertical bars stand for the EFV polymorphic form I.

general, the inconsistency in the morphology of different batches in different dissolution media could arise from different polymorphs as well as the solvent−solute interaction. Dissolution starts with the appearance of the most soluble form and ends with the transformation to a stable form.

FTIR was performed on the residual of EFV-A80 in methanol and EFV-A200 (extreme milling condition) since they show needle-like morphology (Figures 5 and 12f), and the IR spectra were compared with pristine EFV, as shown in Figure 14. EFV revealed the presence of the main characteristic bands of out-of-plane =C−H vibration at 743 cm^{-1}, C−Cl stretching vibration at 1038 cm^{-1}, C−F stretching band at 1000−1400 cm^{-1}, C=C stretching vibration in the aromatic ring at 1601 cm^{-1}, carbonyl group (C=O) stretching at 1745 cm^{-1}, the vibration of alkyne at 2250 cm^{-1}, and N−H stretching at 3300−3400 cm^{-1}.[33] The expected bands in the IR spectrum of EFV-159 (residual in methanol) and EFV-104 were shifted or merged as double or triple peaks revealing the different appearance or molecular shifting around the functional group in the structural orientation compared to pristine EFV. This observation indicates that milling condition's control is essential to avoid unpredictable EFV structure changes.

The selected area electron diffraction (SAED) collected by TEM is shown in Figure 15. Pristine EFV (batch A) shows Debye−Scherrer rings with more prominent spots, indicating that pristine EFV is crystalline and has larger domains than the residual of EFV-A80, which is amorphous after dissolution (Figure 15b). More attention should be devoted to EFV raw material quality and the energy level during the milling process to ensure high milling conditions effectiveness on the EFV drug overall properties.

https://doi.org/10.1021/acsomega.1c00712
ACS Omega 2021, 6, 12647−12659

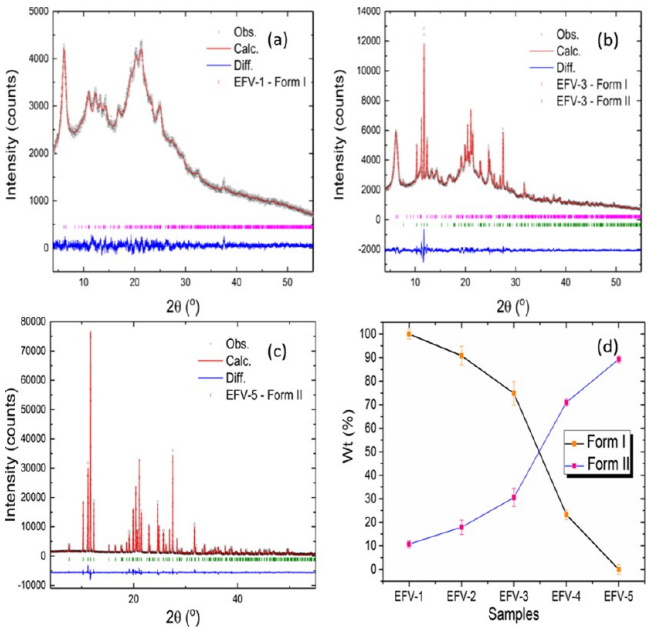

Figure 8. Rietveld refinement plot of (a) EFV-1 (as ground), (b) EFV-3 (after 14 days), (c) EFV-5 (after 60 days), and (d) comparison of EFV polymorphs (form I and II) in wt %. The black circles represent the observed pattern, while the red curve indicates the calculated one. The blue line at the bottom displays the difference between the observed and calculated patterns (residual). The magenta vertical bars stand for the EFV polymorphic form I, while the green vertical bars indicate the EFV polymorphic form II.

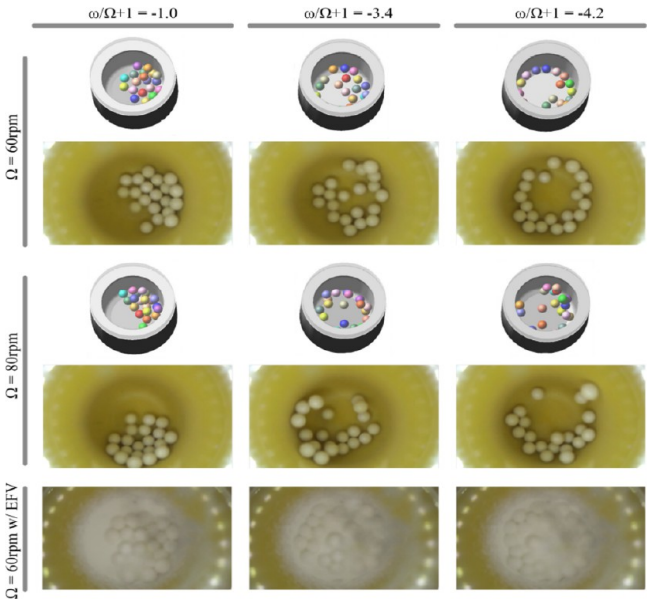

Figure 10. Top and middle, comparison of the camera and simulated images of milling media motion inside the jar for Ω = 60 and 80 rpm, respectively. The maximum disorder of the motion corresponds to $\omega/\Omega + 1 = -3.4$.

The dissolution behavior in distilled water and methanol (Figure 16a−d) is appreciably enhanced in the presence of PVP. Regardless of EFV batches, we observe a reduced agglomeration of the material and a rapid dissolution in the first few minutes. In particular, samples made with main disk speed Ω = 80 rpm (EFV-A80-PVP and EFV-B80-PVP) show a slightly higher dissolution rate in both dissolution media. It is noteworthy that, in the initial points, more rapid dissolution was observed, whereas the final values do not show such a significant increase. PVP thus proves effective in speeding up the early stages of dissolution.

Besides the milling parameters, the nature of the carrier also affects dissolution. PVP has hydrophilic and hydrophobic

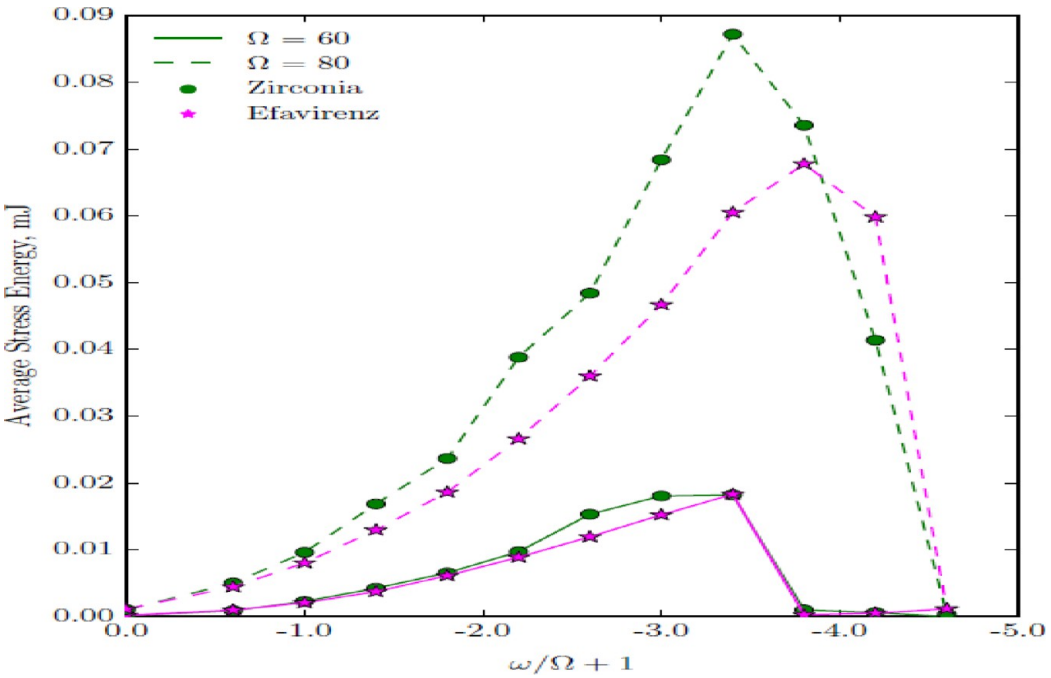

Figure 9. Average stress energy for zirconia−zirconia and zirconia−EFV interactions as a function of the jar to plate angular velocities, computed from simulations performed at Ω = 60 (solid line) and 80 rpm (dashed line). For both the plate velocities and interactions, the maximum location ranges approximately between $\omega/\Omega + 1 = -3.0$ and −3.8.

https://doi.org/10.1021/acsomega.1c00712
ACS Omega 2021, 6, 12647−12659

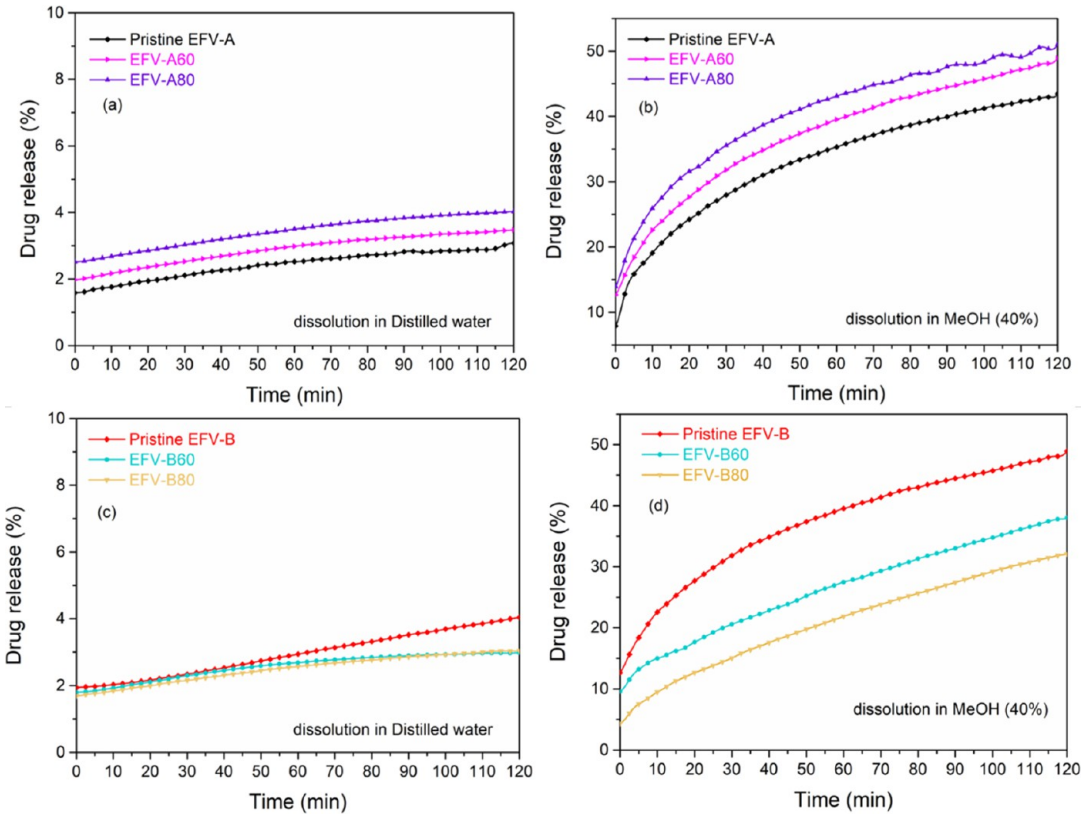

Figure 11. Dissolution profiles of pristine EFV (batch A), EFV-A60 (Ω = 60 rpm), and EFV-A80(Ω = 80 rpm) in (a) distilled water and (b) methanol, and pristine EFV (batch B), EFV-B60 (Ω = 60 rpm), and EFV-B80 (Ω = 80 rpm) in (c) distilled water and (d) methanol.

functional groups, making it easier to interact with EFV and organic and inorganic solvents, such as methanol and water. This enhances the wettability and solubilizing effect via a steric mechanism due to the absorption of the long-chain polymers onto the particles' surfaces, avoiding, therefore, their close approach to enhancing drug solubility and bioavailability. In the absence of PVP, particle dispersions are not sufficiently stable and may coagulate during their formation.

In order to get a clear picture, the SEM morphology of samples containing PVP was studied. The SEM morphology of pristine PVP appears spherical with uneven surfaces (Figure SI-5). The reduction of drug aggregation and agglomeration is evident in PVP-containing EFV samples morphology, regardless of batches (Figure 17 and Figure SI-6−SI-9). EFV particles with irregular shapes formed during milling in PVP presence tend to adsorb on the surface of PVP (Figure 17a,b). The irregular shapes of EFV can increase the wettability, thus reducing the hydrophobicity of EFV.[34] The residual of EFV-PVP in methanol shows different morphological behaviors in different batches. Figure 17c shows that EFV particles almost disappear and PVP particles remain, whereas, in batch B, the EFV particles are still present (Figure 17d). In fact, batch B is more crystalline than A, thus easier to dissolve. In general, PVP polymer interacts with EFV and forms a complex by forming hydrogen bonds between EFV (as hydrogen bond donors) and PVP (as hydrogen bond acceptors), forming a layer around the drug. During the dissolution, the bound EFV can be removed from PVP at the surface by solvent interaction, hence improving the dissolution.

The antiviral activity of different EFV batches and corresponding milled samples was evaluated and is presented in Figure 18. The pristine EFV (batch B) shows a higher ability to inhibit HIV-1 infection than batch A. This is due to the well-crystalline structure of batch B that helps to increase the dissolution. However, milling conditions are more effective on the biological activity of samples prepared based on batch A (EFV-A69 and EFV-A80) and it has less effect on milled samples of batch B. The quality of raw materials (agglomeration and dense particles, amorphous phase) contributes to the milling process's effectiveness and antiviral activity.

As shown in the antiviral activity test, milling significantly reduces the IC50 values of batch A. The performance of EFV-A60 becomes comparable to pristine EFV-B. The significant improvement of the IC50 value for batch A after milling is mainly contributed by the reduced agglomeration of particles and enhanced dissolution rate, in agreement with the dissolution test. Hence, grinding helps improve solubility to minimize the EFV dose to decrease the side effects and costs while preserving the pharmaceutical compound's effectiveness.

3. EXPERIMENTAL SECTION

3.1. Materials. Two batches of EFV were kindly donated by the Brazilian Farmanguinhos-FIOCRUZ, a government pharmaceutical laboratory. These drugs are from the same supplier but different production batches. With this, we intentionally want to consider the variability of the starting material, as it is a common practice with pharmaceutical products, especially when drugs from a known brand are confronted with a generic one with no label. Methanol (99.8%) and polyvinylpyrrolidone (molecular weight = 10,000) were purchased from Sigma Aldrich. For the purpose of analysis,

https://doi.org/10.1021/acsomega.1c00712
ACS Omega 2021, 6, 12647−12659

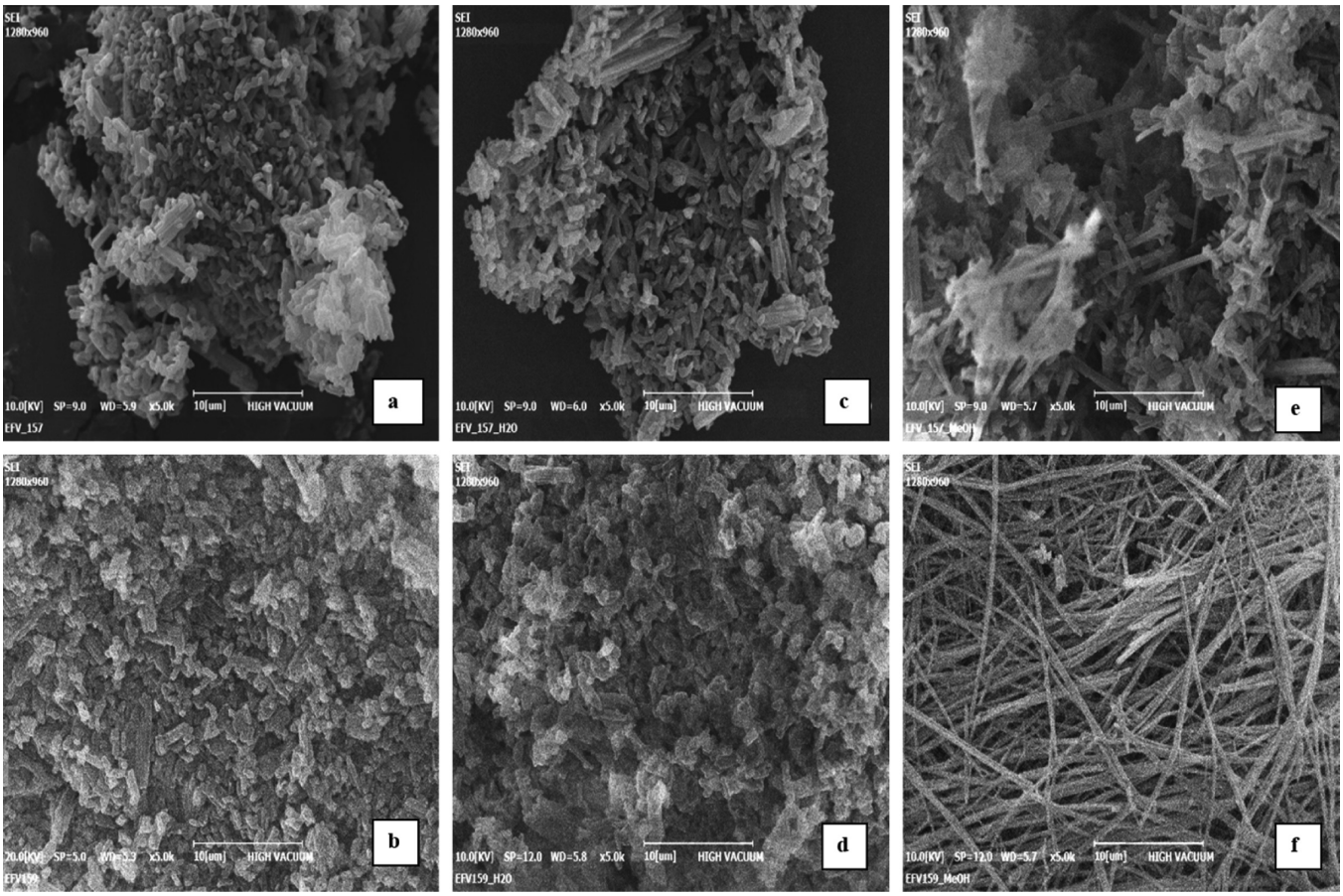

Figure 12. SEM images of (a) as-milled EFV-A60, (b) as-milled EFV-A80, (c) residual of EFV-A60 in distilled water, (d) residual of EFV-A80 in distilled water, (e) residual of EFV-A60 in methanol, and (f) residual of EFV-A80 in methanol.

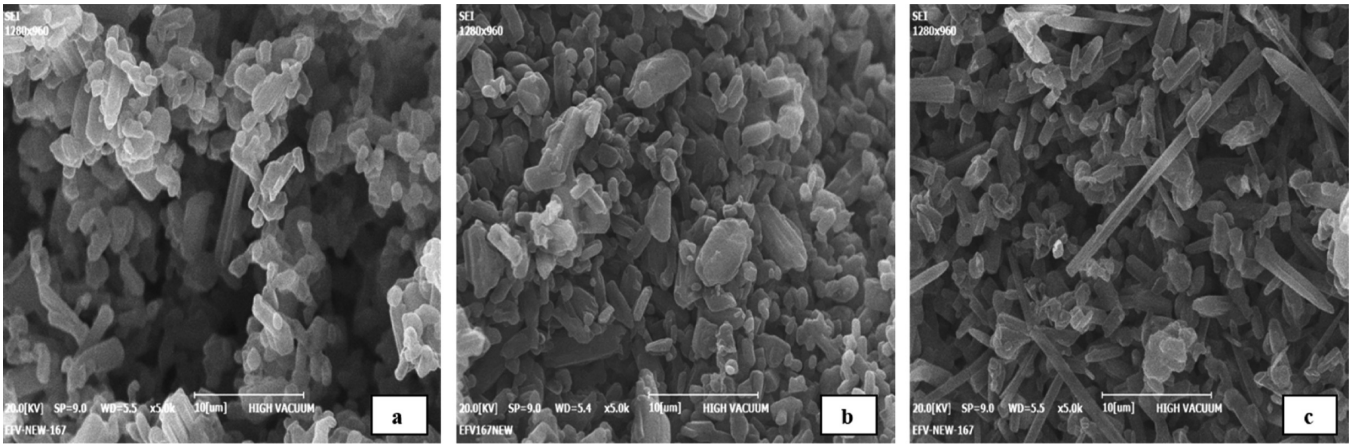

Figure 13. SEM images of (a) as-milled EFV-B60, (b) residual of EFV-B60 in distilled water, and (c) residual of EFV-B60 in methanol.

distilled water was obtained by a purification system Milli-Q (Aquatron A4S).

3.2. Methods. *3.2.1. Sample Preparation.* EFV was subjected to high-energy grinding in a planetary ball mill (Fritsch Pulverisette P4) using zirconium oxide balls and a jar. This material was chosen since it offers at the same time the high grinding efficiency (due to the high density) and great wear resistance, satisfying the requirement of preventing sample contamination, fundamental for the milling of a pharmaceutical. Grinding experiments were performed in a 45 mL jar filled with 20 balls of 3 mm diameter and 800 mg of EFV powder, either with (50 w/w%) and without PVP. The complete set of geometrical and physical properties of the milling media is reported in Table SI-3. Different plate velocities (Ω: 200, 80, and 60) and jar-to-plate velocity ratios ($\omega/\Omega + 1$) were tested by both computer simulations and experiments. In addition, a part of sample preparation was performed at the Federal University of ABC in Brazil, particularly to study the XRPD properties of EFV and ground samples. The samples were ground via a mixer mill MM400 (Retsch, Haan, Germany). Two stainless-steel 10 mL jars and two 10 mm balls were employed. The samples were ball milled

https://doi.org/10.1021/acsomega.1c00712
ACS Omega 2021, 6, 12647−12659

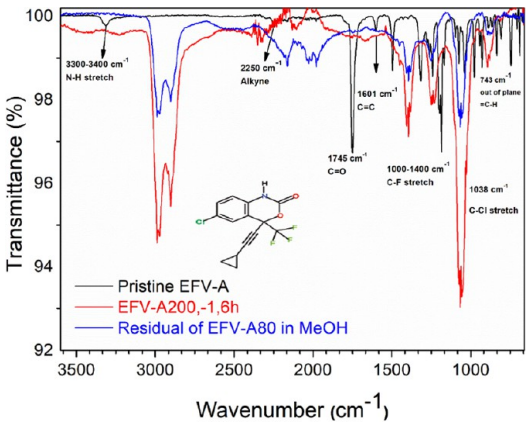

Figure 14. FTIR spectra of efavirenz (batch A), EFV-A200 (Ω = 200 rpm and $\omega/\Omega + 1 = -1$, milling time 6 h), and residual of EFV-A80 in methanol (the inset is the chemical structure of EFV).

at 25 Hz for 5 min with a waiting time of 3 min until reaching 30 min. The same condition was applied to a sample using 1:1 wt % EFV and PVP.

3.2.2. The Multibody Dynamics Model. A multibody dynamics model[35−37] was used for investigating the effect of the jar-(ω) to-plate (Ω) velocity ratio defined as $\omega/\Omega + 1$. Counter-rotating jar and plate are adopted, and, therefore, jar velocity is taken with a negative sign. The case of jar and plate rotating in the same direction was not considered in this study since it has been demonstrated to be less effective in terms of energy transfer and comminution. All the values of parameters adopted for the zirconia−zirconia and zirconia−EFV interactions resulting from the experiments can be found in Table SI-4. Simulations lasting for 24 s were performed for both cases, and the results in terms of relative velocity were exploited to compute the average stress energy.[38] Trajectories of balls were also investigated and compared with camera recordings.

3.2.3. Camera Recordings. The balls motion[38] was monitored *in operando* by means of a high-speed camera (Sony Action Cam HDR-AS200V, 240 fps, 1280 × 720 pixel resolution) both with and without the EFV mill charge, by installing the equipment. Since the camera was directly installed on the jar through an expressly designed slot, the recorded balls' trajectories refer to the vial reference frame. The visibility of milling media was allowed by a transparent polycarbonate lid and 50 LEDs mounted on a ring (i.e., an automotive angel eye). The first group of recordings was taken without the mill feed, and then calcium fluoride was added for a new batch of observations. This way, the effect of the mill charge was clearly highlighted. Camera recordings allowed a qualitative comprehension of balls' movements and their dependence on milling parameters setup.

3.3. Characterization. X-ray powder diffraction (XRPD) patterns of pristine EFV (batch A and B) were obtained using a Panalytical X'Pert MRD instrument (Philips) equipped with a Co Kα radiation (λ = 1.7889 Å) sealed tube operated at 40 kV and 40 mA; the XRPD patterns of ball-milled EFV were recorded using a Thermo-ARL X'TRA diffractometer with Mo Kα radiation (λ = 0.7093 Å) generated at 50 kV and 40 mA, with a scanning rate of 0.4°/min over the 1.5−12° 2θ range. Measurements were performed in Bragg−Brentano geometry. The analysis of each powder pattern under the whole powder pattern modeling (WPPM) approach,[39−41] provided with the corresponding full width at half maximum (FWHM), which in the present context can be taken as inversely proportional to the size of the crystalline domains.[42] In addition, some of XRPD data were collected in transmission geometry using a STADI-P (Stoe, Darmstadt, Germany) diffractometer equipped with a Ge(111) primary beam monochromator, providing pure Cu Kα_1 radiation (λ = 1.54056 Å), and operating at 40 kV and 40 mA. The samples were loaded between two cellulose acetate foils, and the sample holder was kept spinning during data collection. The X-ray photons were detected using a linear detector, Mythen 1 K (Dectris, Baden, Switzerland). The measurements were carried out in the 2θ region from 4° to 55.935° in steps of 0.015° and a counting time of 100 s at each 1.05°. To calculate the samples' degree of crystallinity in TOPAS-Academic V7, two peaks (Peaks_Phase; the peaks were positioned at 2θ values of 12.1° and 20.6°) were inserted to perform single line fittings, from sample EFV to EFV-5. Their corresponding peak positions and areas were then maintained fixed to obtain the samples' amorphous contribution. The "degree of crystallinity-DoC" was obtained taking into account the calculated "total area" that contributed to the overall diffraction pattern, i.e., the full areas under the amorphous contribution (inferred as the broadening due to the two peaks inserted in the diffraction patterns) and the ones due to the crystalline phases of both form I and/or form II. Transmission electron microscopy (TEM) imaging and selected area electron diffraction (SAED) were performed with a high-resolution scanning/transmission electron microscopy instrument (Thermo Fisher TALOS 200 s). The measurements have been carried out at an accelerating voltage

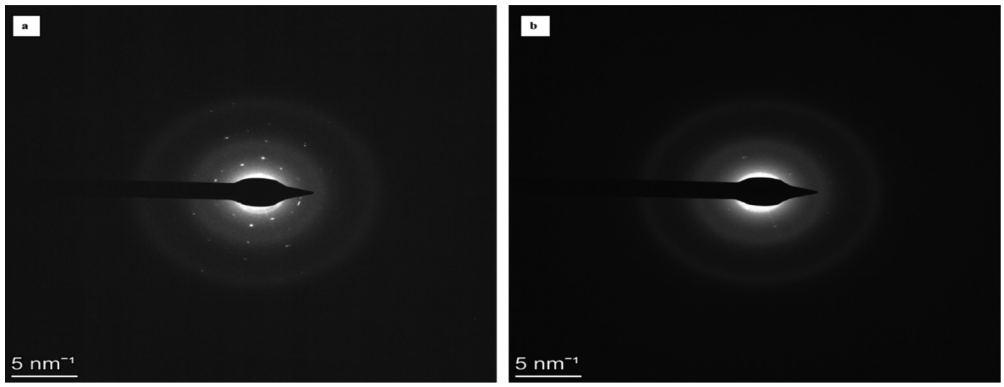

Figure 15. SAED pattern of (a) pristine EFV (batch A) and (b) residual of EFV-A80 in methanol.

https://doi.org/10.1021/acsomega.1c00712
ACS Omega 2021, 6, 12647−12659

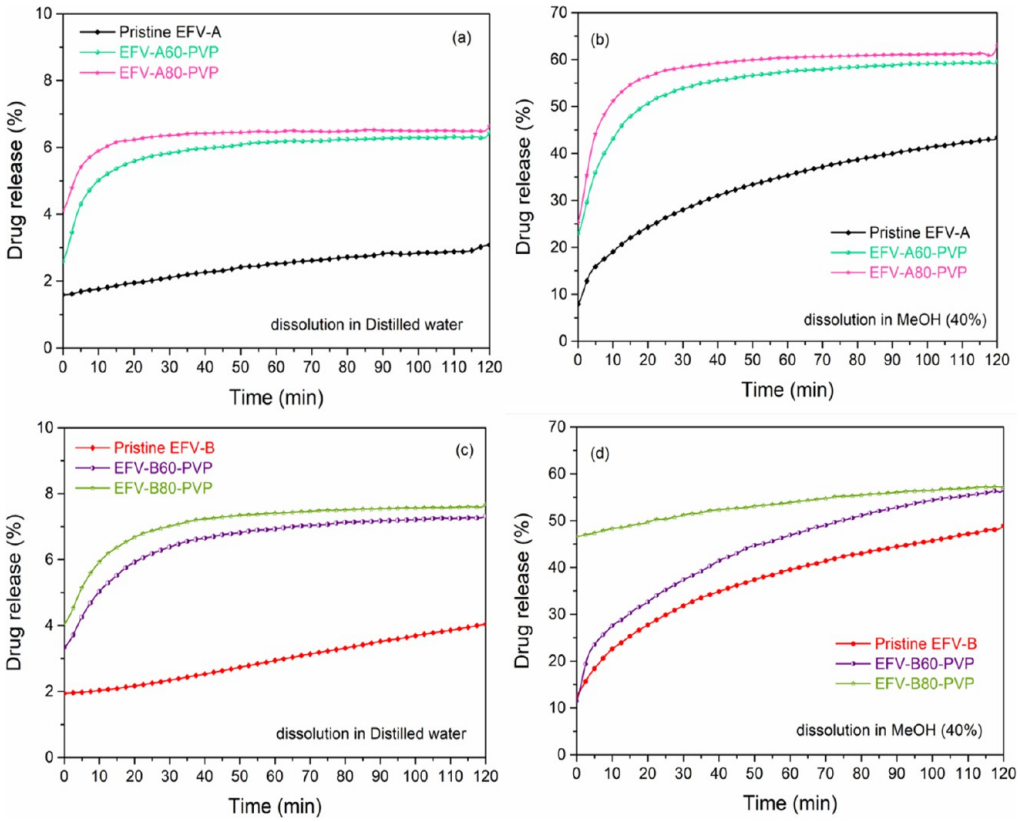

Figure 16. Dissolution profiles of pristine EFV (batch A), EFV-A60-PVP, and EFV-A80-PVP in (a) distilled water and (b) methanol, and pristine-EFV (batch B), EFV-B60-PVP, and EFV-B80-PVP in (c) distilled water and (d) methanol.

of 200 kV. The dissolution test was performed on powder samples using an Erweka DT-626 dissolution tester. (six vessels) with a paddle apparatus. The dissolution procedure consisted of placing 100 mg of the drug (powder) into the dissolution vessel. Dissolution conditions were 900 mL of methanol solution (40% V/V) kept at constant human body temperature (37.0 ± 0.5 °C) with a rotation speed of 50 rpm. The drug release in the dissolution media was real-time measured using a UV−vis spectrophotometer (Perkin Elmer Lambda 750) coupled with the dissolutor. Samples were collected after 10 s required for the drug to disintegrate and release continuously using a 40 μm cannula filter; the analysis was performed at 248 nm wavelength. The same procedure was performed for the distilled water. A scanning electron microscope was utilized to visualize the samples' grain shape and surface morphology using a Coxem EM-30AX instrument. For SEM observations, all samples were coated with a Au−Pd (25 mA) metallization layer. Fourier transform infrared spectroscopy (FTIR) was performed using a Perkin Elmer spectrometer by averaging 16 scans with a resolution of 2 cm^{-1} in the wavenumber range between 650 and 4000 cm^{-1}.[43] The samples' biological activity was assessed using single-round HIV-1 Env-defective HIV-1 (NL4-3) complemented with Env derived from HIV-1 HXB2 expressed with the vector PBJ5. Viral particles were harvested 48 h post-transfection, clarified by low-speed centrifugation at 300 g for 5 min, and filtered through a 0.45 μm pore filter.[44] At 30 mM, stock solutions were prepared in 50/50% ethanol/milli-Q water for all 10 samples of efavirenz. Stock solutions were further diluted to obtain a final concentration of 30 nM in complete DMEM, supplemented with 1% glutamine (Gibco), and 10% heat-inactivated fetal bovine serum (FBS) (Gibco) containing HIV NL4-3. Preliminary tests were performed to determine the optimal concentration range of efavirenz to determine the IC50 value. TZM-bl stably transfected with a construct containing ZsGreen fluorescent protein expressed under the control of HIV LTR[45] were seeded 1 day prior to infection at a density of 20 k cells/well in a 96-well plate (Corning) in complete DMEM. Right before efavirenz administration, the culture medium was replaced with complete DMEM containing HIV-1 NL4-3. Efavirenz dilutions were added to the plate, and serial dilutions 1:3 were performed in triplicate. Seven concentrations were tested to determine IC50 values for each sample. The number of positive (infected) cells was measured using an EnSight multimode plate reader (Perkin Elmer) (excitation 465 nm), normalized on control (untreated cells exposed to NL4-3), and expressed as a percentage; these data were fitted with a sigmoidal a curve using the least square variable slope method and the dose-normalized response with GraphPad to determine the IC50 value for each sample.

4. CONCLUSIONS

This study proved that ball milling is a convenient tool to improve the dissolution rate of EFV. The extreme grinding condition (Ω = 200 rpm) with a long milling time (6 h) results in recrystallization and agglomeration of EFV, associated with a decrease in solubility. In addition, the decrease in crystalline domain size does not imply an improvement of the dissolution behavior, which not only depends on the size and shape of the crystals but also on the agglomeration grade of efavirenz raw materials.

https://doi.org/10.1021/acsomega.1c00712
ACS Omega 2021, 6, 12647−12659

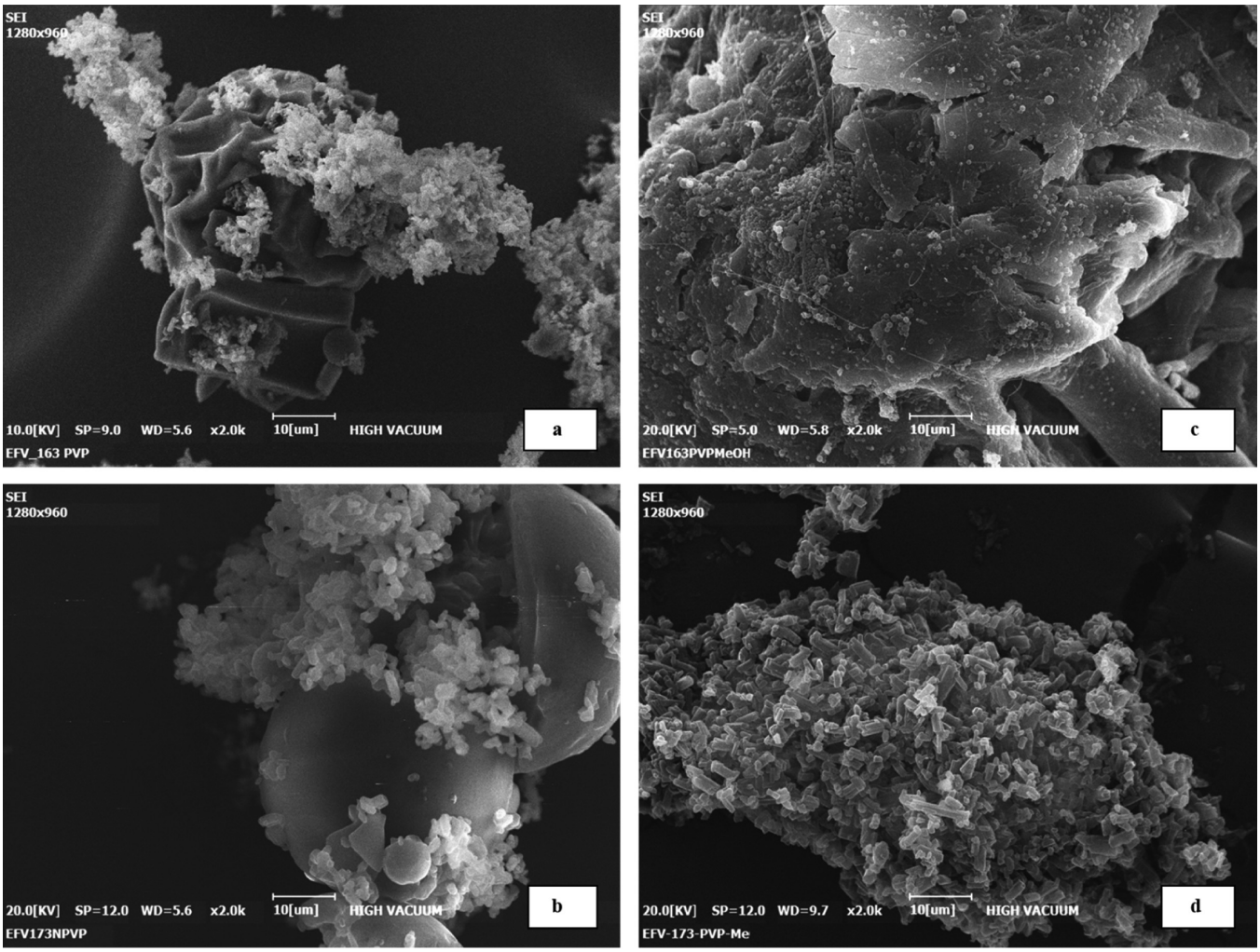

Figure 17. SEM images of (a) as-milled EFV-A80-PVP (Ω = 80 rpm), (b) as-milled EFV-B80-PVP (Ω = 80 rpm), (c) residual of EFV-A80-PVP in methanol, and (d) residual of EFV-B80-PVP in methanol.

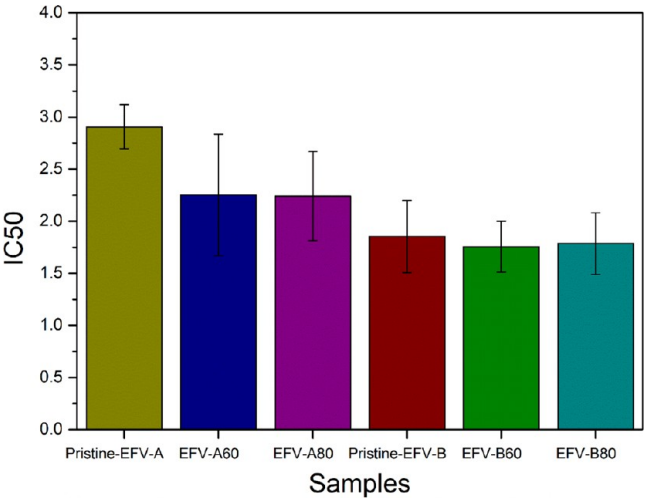

Figure 18. HIV-1 NL4-3 inhibition of different batches of EFV and the ground samples under different conditions. IC50 values are calculated from fitted sigmoidal dose−response curves, as described in the Methods section. Error bars represent the standard deviations of the mean calculated from several independent experiments.

Therefore, an optimization of grinding variables was performed via a multibody dynamics model. The experimental results proved that milling conditions' effectiveness is significantly dependent on the quality of pristine EFV materials. The starting material with a well-crystalline structure (batch B) shows a higher dissolution rate both in distilled water and in methanol (40%) with respect to as-milled samples and batch A. The reduction of energy (Ω) to 80 rpm and time to 30 min (non-stop) was found to effectively enhance the dissolution of batch A, with favorable results obtained in methanol. This milling condition reduces the agglomerated and dense particles of EFV while essentially keeping intact its crystalline nature.

It was found that the combination of PVP with EFV markedly enhances the dissolution rate of efavirenz. In fact, the improvements of dissolution using PVP could be explained by forming a hydrophilic layer on the surface of EFV, resulting in the drug's wettability and stabilization. The stabilization of such complexes is due to a cooperative interaction through hydrogen bonds forming between EFV (as hydrogen bond donors) and PVP (as hydrogen bond acceptors) groups on the polymer chain. In addition, the morphology of the samples following the grinding was studied. A detailed study of the morphology of the EFV residual in different media (distilled water and methanol) indicates the presence of different

https://doi.org/10.1021/acsomega.1c00712
ACS Omega 2021, 6, 12647−12659

polymorphs in EFV. A gradual transformation of the EFV polymorph (from form I to II) was monitored by XRPD and correlated with the dissolution phenomena and morphological behavior. The antiviral activity is affected by the pristine EFV quality, specifically its microstructural properties or agglomeration grade. Batch B shows a higher ability to inhibit HIV-1 infection than batch A, requiring a decreased dosage to achieve therapeutic levels in the body. In general, high-energy grinding is more effective on EFV materials containing a small degree of amorphous phase; hence more attention should be devoted to the quality of the pristine EFV material and to the energy level during the milling process to ensure the effectiveness of milling on the overall properties of the EFV drug.

■ ASSOCIATED CONTENT

Supporting Information

The Supporting Information is available free of charge at https://pubs.acs.org/doi/10.1021/acsomega.1c00712.

> The fitting results of Rietveld refinements and Rietveld plot of EFV and ball-milled EFV samples; XRPD pattern of EFV contained PVP; dissolution profile of as-milled EFV under extreme milling conditions; the weight of EFV residual in distilled water and methanol; SEM images of pristine PVP, as-milled EFV (batch A and B), and their residuals in distilled water and methanol with and without PVP; geometrical and physical properties of jar and milling media for the case study of EFV grinding; parameters used for the contact and the friction models and method used for their derivation (PDF)

■ AUTHOR INFORMATION

Corresponding Author

Narges Ataollahi − *Department of Civil, Environmental and Mechanical Engineering, University of Trento, Trento 38123, Italy*; orcid.org/0000-0002-8135-6054; Email: narges.ataollahi@unitn.it

Authors

Marica Broseghini − *Helmholtz Zentrum Geesthacht (HZG), Institute of Coastal Research, Geesthacht 21502, Germany*

Fabio F. Ferreira − *Center for Natural and Human Sciences, Federal University of ABC, Santo André, SP 09210-580, Brazil*; orcid.org/0000-0003-1516-1221

Alberto Susana − *Centre for Integrative Biology, University of Trento, Trento 38123, Italy*

Massimo Pizzato − *Centre for Integrative Biology, University of Trento, Trento 38123, Italy*

Paolo Scardi − *Department of Civil, Environmental and Mechanical Engineering, University of Trento, Trento 38123, Italy*; orcid.org/0000-0003-1097-3917

Complete contact information is available at: https://pubs.acs.org/10.1021/acsomega.1c00712

Author Contributions

The manuscript was written through contributions of all authors. All authors have given approval to the final version of the manuscript.

Notes

The authors declare no competing financial interest.

■ ACKNOWLEDGMENTS

The authors would like to acknowledge Dr. Mirco D'incau, Dr. Elisa Cappelletto, Dr. Eleonora Isotta, and Dr. Ketan Lohani for all their help in this study. F.F.F. acknowledges the financial support provided by the National Council for Scientific and Technological Development (CNPq proc. #305601/2019-9, Brazil).

■ REFERENCES

(1) Taneja, S.; Shilpi, S.; Khatri, K. Formulation and Optimization of Efavirenz Nanosuspensions Using the Precipitation-Ultrasonication Technique for Solubility Enhancement. *Artif. Cells, Nanomed., Biotechnol.* **2015**, *44*, 978−984.

(2) Fandaruff, C.; Rauber, G. S.; Araya-Sibaja, A. M.; Pereira, R. N.; De Campos, C. E. M.; Rocha, H. V. A.; Monti, G. A.; Malaspina, T.; Silva, M. A. S.; Cuffini, S. L. Polymorphism of Anti-HIV Drug Efavirenz: Investigations on Thermodynamic and Dissolution Properties. *Cryst. Growth Des.* **2014**, *14*, 4968−4975.

(3) Cappelletto, E.; Firrito, C.; Pizzato, M.; Rebuffi, L.; Scardi, P. Mechanical Activation of Efavirenz: The Effects on the Dissolution and Inhibitory Behavior. *Pharm. Dev. Technol.* **2018**, *23*, 1128−1135.

(4) Savjani, K. T.; Gajjar, A. K.; Savjani, J. K. Drug Solubility: Importance and Enhancement Techniques. *ISRN Pharm.* **2012**, *2012*, 1−10.

(5) Beers, M.; Porter, R.; Jones, T.; Kaplan, J.; Berkwits, M. *The Merck Manual of Diagnosis and Therapy*; 18th ed.; Merck Research Laboratories: Whitehouse Station, N.J., 2006.

(6) Maurin, M. B.; Rowe, S. M.; Blom, K.; Pierce, M. E. Kinetics and Mechanism of Hydrolysis of Efavirenz. *Pharm. Res.* **2002**, *19*, 517−521.

(7) Cristofoletti, R.; Nair, A.; Abrahamsson, B.; Groot, D. W.; Kopp, S.; Langguth, P.; Polli, J. E.; Shah, V. P.; Dressman, J. B. Biowaiver Monographs for Immediate Release Solid Oral Dosage Forms: Efavirenz. *J. Pharm. Sci.* **2013**, *102*, 318−329.

(8) Costa, B. L. A.; Sauceau, M.; Del Confetto, S.; Sescousse, R.; Ré, M. I. Determination of Drug-Polymer Solubility from Supersaturated Spray-Dried Amorphous Solid Dispersions: A Case Study with Efavirenz and Soluplus. *Eur. J. Pharm. Biopharm.* **2019**, *142*, 300−306.

(9) De Melo, A. C. C.; De Amorim, I. F.; Cirqueira, M. D. L.; Martins, F. T. Toward Novel Solid-State Forms of the Anti-HIV Drug Efavirenz: From Low Screening Success to Cocrystals Engineering Strategies and Discovery of a New Polymorph. *Cryst. Growth Des.* **2013**, *13*, 1558−1569.

(10) Da Costa, M. A.; Seiceira, R. C.; Rodrigues, C. R.; Hoffmeister, C. R. D.; Cabral, L. M.; Rocha, H. V. A. Efavirenz Dissolution Enhancement I: Co-Micronization. *Pharmaceutics* **2013**, *5*, 1−22.

(11) Khadka, P.; Ro, J.; Kim, H.; Kim, I.; Kim, J. T.; Kim, H.; Cho, J. M.; Yun, G.; Lee, J. Pharmaceutical Particle Technologies: An Approach to Improve Drug Solubility, Dissolution and Bioavailability. *Asian J. Pharm. Sci.* **2014**, *9*, 304−316.

(12) Belgamwar, A.; Khan, S.; Yeole, P. Intranasal Chitosan-g-HPβCD Nanoparticles of Efavirenz for the CNS Targeting. *Artif. Cells, Nanomed., Biotechnol.* **2018**, *46*, 374−386.

(13) Madhavi, B. B.; Kusum, B.; Chatanya, C. K.; Madhu, M. N.; Harsha, V. S.; Banji, D. Dissolution Enhancement of Efavirenz by Solid Dispersion and PEGylation Techniques. *Int. J. Pharm. Investig.* **2011**, *1*, 29.

(14) Alves, L. D. S.; De La Roca Soares, M. F.; De Albuquerque, C. T.; Da Silva, É. R.; Vieira, A. C. C.; Fontes, D. A. F.; Figueirêdo, C. B. M.; Soares Sobrinho, J. L.; Rolim Neto, P. J. Solid Dispersion of Efavirenz in PVP K-30 by Conventional Solvent and Kneading Methods. *Carbohydr. Polym.* **2014**, *104*, 166−174.

(15) Teodorescu, M.; Bercea, M. Poly(Vinylpyrrolidone) − A Versatile Polymer for Biomedical and Beyond Medical Applications. *Polym.-Plast. Technol. Eng.* **2015**, *54*, 923−943.

(16) da Costa, M.; Lione, V. O.; Rodrigues, C.; Cabra, L.; Rocha, H. V. Efavirenz Dissolution Enhancement II:Aqueous Co-Spray-Draying

| International Journal of Pharmaceutical Sciences and Research. *Int. J. Pharm. Sci. Res.* **2015**, 3807−3820.
(17) Pawar, J.; Tayade, A.; Gangurde, A.; Moravkar, K.; Amin, P. Solubility and Dissolution Enhancement of Efavirenz Hot Melt Extruded Amorphous Solid Dispersions Using Combination of Polymeric Blends: A QbD Approach. *Eur. J. Pharm. Sci.* **2016**, *88*, 37−49.
(18) Pawar, J. N.; Fule, R. A.; Maniruzzaman, M.; Amin, P. D. Solid Crystal Suspension of Efavirenz Using Hot Melt Extrusion: Exploring the Role of Crystalline Polyols in Improving Solubility and Dissolution Rate. *Mater. Sci. Eng.: C* **2017**, *78*, 1023−1034.
(19) Loh, Z. H.; Samanta, A. K.; Sia Heng, P. W. Overview of Milling Techniques for Improving the Solubility of Poorly Water-Soluble Drugs. *Asian J. Pharm. Sci.* **2015**, *10*, 255−274.
(20) Junyaprasert, V. B.; Morakul, B. Nanocrystals for Enhancement of Oral Bioavailability of Poorly Water-Soluble Drugs. *Asian J. Pharm. Sci.* **2015**, *10*, 13−23.
(21) Dizaj, S. M.; Vazifehasl, Z.; Salatin, S.; Adibkia, K.; Javadzadeh, Y. Nanosizing of Drugs: Effect on Dissolution Rate. *Res. Pharm. Sci.* **2015**, *10*, 95−108.
(22) Dokoumetzidis, A.; Macheras, P. A Century of Dissolution Research: From Noyes and Whitney to the Biopharmaceutics Classification System. *Int. J. Pharm.* **2006**, *321*, 1−11.
(23) Sinha, B.; Müller, R. H.; Möschwitzer, J. P. Bottom-up Approaches for Preparing Drug Nanocrystals: Formulations and Factors Affecting Particle Size. *Int. J. Pharm.* **2013**, *453*, 126−141.
(24) Chang, T.-L.; Zhan, H.; Liang, D.; Liang, J. F. Nanocrystal Technology for Drug Formulation and Delivery. *Front. Chem. Sci. Eng.* **2015**, *9*, 1−14.
(25) Rasenack, N.; Müller, B. W. Micron-Size Drug Particles: Common and Novel Micronization Techniques. *Pharm. Dev. Technol.* **2004**, *9*, 1−13.
(26) Cappelletto, E.; Rebuffi, L.; Flor, A.; Scardi, P. Microstructural Effects of High-Energy Grinding on Poorly Soluble Drugs: The Case Study of Efavirenz. *Powder Diffr.* **2017**, *32*, S135−S140.
(27) Mahapatra, S.; Thakur, T. S.; Joseph, S.; Varughese, S.; Desiraju, G. R. New Solid State Forms of the Anti-HIV Drug Efavirenz. Conformational Flexibility and High Z′ Issues. *Cryst. Growth Des.* **2010**, *10*, 3191−3202.
(28) Bruno, I. J.; Cole, J. C.; Edgington, P. R.; Kessler, M.; Macrae, C. F.; McCabe, P.; Pearson, J.; Taylor, R. New Software for Searching the Cambridge Structural Database and Visualizing Crystal Structures. *Acta Crystallogr., Sect. B: Struct. Sci.* **2002**, *58*, 389−397.
(29) Coelho, A. A. TOPAS and TOPAS-Academic: An Optimization Program Integrating Computer Algebra and Crystallographic Objects Written in C++: An. *J. Appl. Crystallogr.* **2018**, *51*, 210−218.
(30) Ravikumar, K.; Sridhar, B. Molecular and Crystal Structure of Efavirenz, a Potent and Specific Inhibitor of HIV-1 Reverse Transcriptase, and Its Monohydrate. *Mol. Cryst. Liq. Cryst.* **2009**, *515*, 190−198.
(31) Hernandez, C. C.; Ferreira, F. F.; Rosa, D. S. X-Ray Powder Diffraction and Other Analyses of Cellulose Nanocrystals Obtained from Corn Straw by Chemical Treatments. *Carbohydr. Polym.* **2018**, *193*, 39−44.
(32) Hill, R. J.; Howard, C. J. Quantitative Phase Analysis from Neutron Powder Diffraction Data Using the Rietveld Method. *J. Appl. Crystallogr.* **1987**, *20*, 467−474.
(33) Gomes, E. C. d. L.; Mussel, W. N.; Resende, J. M.; Fialho, S. L.; Barbosa, J.; Yoshida, M. I. Chemical Interactions Study of Antiretroviral Drugs Efavirenz and Lamivudine Concerning the Development of Stable Fixed-Dose Combination Formulations for AIDS Treatment. *J. Braz. Chem. Soc.* **2013**, *24*, 573−579.
(34) Fitriani, L.; Haqi, A.; Zaini, E. Preparation and Characterization of Solid Dispersion Freeze-Dried Efavirenz - Polyvinylpyrrolidone K-30. *J. Adv. Pharm. Technol. Res.* **2016**, *7*, 105−109.
(35) Broseghini, M.; Gelisio, L.; D'Incau, M.; Azanza Ricardo, C. L.; Pugno, N. M.; Scardi, P. Modeling of the Planetary Ball-Milling Process: The Case Study of Ceramic Powders. *J. Eur. Ceram. Soc.* **2016**, *36*, 2205−2212.
(36) Broseghini, M.; D'Incau, M.; Gelisio, L.; Pugno, N. M.; Scardi, P. Effect of Jar Shape on High-Energy Planetary Ball Milling Efficiency: Simulations and Experiments. *Mater. Des.* **2016**, *110*, 365−374.
(37) Broseghini, M.; D'Incau, M.; Gelisio, L.; Pugno, N. M.; Scardi, P. Homogeneity of Ball Milled Ceramic Powders: Effect of Jar Shape and Milling Conditions. *Data Brief* **2017**, *10*, 186−191.
(38) Broseghini, M.; D'Incau, M.; Gelisio, L.; Pugno, N. M.; Scardi, P. Numerical and Experimental Investigations on New Jar Designs for High Efficiency Planetary Ball Milling. *Adv. Powder Technol.* **2020**, *31*, 2641−2649.
(39) Scardi, P. Chapter 13. Microstructural Properties: Lattice Defects and Domain Size Effects. In *Powder Diffraction; Royal Society of Chemistry*; 2008; pp. 376−413.
(40) Scardi, P.; Leoni, M. Diffraction Line Profiles from Polydisperse Crystalline Systems. Corrigenda. *Acta Crystallogr., Sect. A: Found. Crystallogr.* **2001**, *57*, 604−613.
(41) Scardi, P.; Leoni, M. Whole Powder Pattern Modelling. *Acta Crystallogr. Sect. A Found. Crystallogr.* **2002**, *58*, 190−200.
(42) Klug, H. P.; Alexander, L. E. *X-Ray Diffraction Procedures: For Polycrystalline and Amorphous Materials, 2nd Edition | Wiley*; 2nd ed.; Wiley-Interscience: 1974.
(43) Ataollahi, N.; Ahmad, A.; Hamzah, H.; Rahman, M. Y. A.; Mohamed, N. S. Ionic Conductivity of PVDF-HFP/MG49 Based Solid Polymer Electrolyte. In *Advanced Materials Research*; Trans Tech Publications Ltd: 2012; Vol. *501*, pp. 29−33.
(44) Pizzato, M.; Helander, A.; Popova, E.; Calistri, A.; Zamborlini, A.; Palù, G.; Göttlinger, H. G. Dynamin 2 Is Required for the Enhancement of HIV-1 Infectivity by Nef. *Proc. Natl. Acad. Sci.* **2007**, *104*, 6812−6817.
(45) Rosa, A.; Chande, A.; Ziglio, S.; De Sanctis, V.; Bertorelli, R.; Goh, S. L.; McCauley, S. M.; Nowosielska, A.; Antonarakis, S. E.; Luban, J.; Santoni, F. A.; Pizzato, M. HIV-1 Nef Promotes Infection by Excluding SERINC5 from Virion Incorporation. *Nature* **2015**, *526*, 212−217.

https://doi.org/10.1021/acsomega.1c00712
ACS Omega 2021, 6, 12647−12659